ARMY RESEARCH LABORATORY

Effect of Impurities on the Electronic Structure of Grain Boundaries and Intergranular Cohesion in Tungsten

Genrich L. Krasko

ARL-TR-685 February 1995

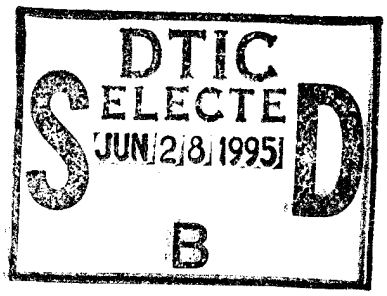

19950627 053

DTIC QUALITY INSPECTED 5

Approved for public release; distribution unlimited.

The findings in this report are not to be construed as an official Department of the Army position unless so designated by other authorized documents.

Citation of manufacturer's or trade names does not constitute an official endorsement or approval of the use thereof.

Destroy this report when it is no longer needed. Do not return it to the originator.

REPORT DOCUMENTATION PAGE

Form Approved
OMB No. 0704-0188

Public reporting burden for this collection of information is estimated to average 1 hour per response, including the time for reviewing instructions, searching existing data sources, gathering and maintaining the data needed, and completing and reviewing the collection of information. Send comments regarding this burden estimate or any other aspect of this collection of information, including suggestions for reducing this burden, to Washington Headquarters Services, Directorate for Information Operations and Reports, 1215 Jefferson Davis Highway, Suite 1204, Arlington, VA 22202-4302, and to the Office of Management and Budget, Paperwork Reduction Project (0704-0188), Washington, DC 20503.

1. AGENCY USE ONLY *(Leave blank)*	2. REPORT DATE	3. REPORT TYPE AND DATES COVERED
	February 1995	Progress FY93 - FY94

4. TITLE AND SUBTITLE Effect of Impurities on the Electronic Structure of Grain Boundaries and Intergranular Cohesion in Tungsten

5. FUNDING NUMBERS

6. AUTHOR(S)

Genrich L. Krasko

7. PERFORMING ORGANIZATION NAME(S) AND ADDRESS(ES)

Army Research Laboratory
Watertown, MA 02172-0001
ATTN: AMSRL-MA-CC

8. PERFORMING ORGANIZATION REPORT NUMBER

ARL-TR-685

9. SPONSORING/MONITORING AGENCY NAME(S) AND ADDRESS(ES)

10. SPONSORING/MONITORING AGENCY REPORT NUMBER

11. SUPPLEMENTARY NOTES

12a. DISTRIBUTION/AVAILABILITY STATEMENT

Approved for public release; distribution unlimited.

12b. DISTRIBUTION CODE

13. ABSTRACT *(Maximum 200 words)*

Abstract: The cohesion of a grain boundary (GB) is believed to be the controlling factor limiting the ductility of high-strength metallic alloys, and particularly those containing W. Intergranular embrittlement is usually associated with segregation of impurities at the GBs. Impurities present in ppm concentrations can result in a dramatic decrease in plasticity. This paper reviews recent results on both semi-empirical and first-principles modelling of the energetics and the electronic structures of impurities on a $\Sigma 3$ (111) GB in W. Our calculations have shown that impurities, such as N, O, P, S, and Si, weaken the intergranular cohesion resulting in 'loosening' of the GB. The presence of B and C on the contrary, enhances the interatomic interaction across the GB. The so-called 'site-competition effect' should play an important role affecting impurity distribution in W GBs. Among the impurities analyzed, B in the GB has the lowest energy and thus would tend to displace other impurity atoms from the GB. Microalloying with 10–50 ppm B may be an effective way of improving tungsten's ductility. These results are important for understanding the fundamental physics of intergranular embrittlement.

14. SUBJECT TERMS	15. NUMBER OF PAGES
Grain Boundary, Electronic Structure, Cohesion, Tungsten	13
	16. PRICE CODE

17. SECURITY CLASSIFICATION OF REPORT	18. SECURITY CLASSIFICATION OF THIS PAGE	19. SECURITY CLASSIFICATION OF ABSTRACT	20. LIMITATION OF ABSTRACT
Unclassified	Unclassified	Unclassified	UL

ELSEVIER

Int. J. of Refractory Metals & Hard Materials **12** (1993–1994) 251–260
Elsevier Science Limited
Printed in Great Britain
0263-4368/94/$7.00

Effect of Impurities on the Electronic Structure of Grain Boundaries and Intergranular Cohesion in Tungsten

Genrich L. Krasko

Metals Division, US Army Research Laboratory, Watertown, MA 02172-0001, USA

(Received 1 July 1993; accepted 8 September 1993)

Abstract: The cohesion of a grain boundary (GB) is believed to be the controlling factor limiting the ductility of high-strength metallic alloys, and particularly those containing W. Intergranular embrittlement is usually associated with segregation of impurities at the GBs. Impurities present in ppm concentrations can result in a dramatic decrease in plasticity. This paper reviews recent results on both semi-empirical and first-principles modelling of the energetics and the electronic structures of impurities on a Σ3 (111) GB in W. Our calculations have shown that impurities, such as N, O, P, S, and Si, weaken the intergranular cohesion resulting in 'loosening' of the GB. The presence of B and C on the contrary, enhances the interatomic interaction across the GB. The so-called 'site-competition effect' should play an important role affecting impurity distribution in W GBs. Among the impurities analyzed, B in the GB has the lowest energy and thus would tend to displace other impurity atoms from the GB. Microalloying with 10–50 ppm B may be an effective way of improving tungsten's ductility. These results are important for understanding the fundamental physics of intergranular embrittlement.

INTRODUCTION

The reduced cohesion of grain boundaries (GBs) is often the controlling factor limiting ductility, and hence performance and reliability of high-strength metallic alloys.[1] Intergranular embrittlement in metals is usually caused by impurities segregating towards the GBs.[2–6a] A ductile–brittle transition temperature (DBTT) as low as −196°C[7] was observed in high-purity W single crystals obtained by electron-beam zone-melting with impurity gettering. Impurities present in bulk concentrations of only 10^{-3}–10^{-4} atomic percent can result in a dramatic decrease in plasticity. This drastic degradation of mechanical properties of metallic alloys, in particular W, poses significant technological and application problems. This detrimental effect of minute impurity concentrations can be readily understood: a ppm amount of impurity is sufficient for saturating all the GBs in a polycrystal of a typical grain size. Sensitivity of the DBTT to the grain size confirms the above physical concept: the larger the grain size, the smaller is the amount of impurity needed to saturate the GB.[3] Finer-grain polycrystals are known to be less brittle. For a Σ3 (111) GB in a W BCC crystal, Table 1 shows the estimated amounts of impurities sufficient to create a monolayer coating.

Brittle fracture is inherently related to the nucleation and propagation of cracks. In this paper, however, we shall focus exclusively on the microscopic aspects of embrittlement; the role of impurities will therefore be considered only from the point of view of their effect on intergranular cohesion as the main factor controlling ductile/brittle behavior.

If the presence of impurities is so detrimental, gettering these impurities is an obvious way of ductilizing W. A well-known, though extremely costly, option is to use the so-called 'Rhenium Effect' (see, for example, Ref. 8). A more promising way of removing the 'harmful' impurities, such

Table 1. Amounts of impurity atoms sufficient for forming a monolayer in the GB

Grain size (μm)	5	10	20	50	100
Amount of impurity (atomic ppm)	60	30	15	6	3

as O, N, P, from the GBs is by gettering where these form thermodynamically stable phases with other elements, e.g. Ti, Y, Mo, Zr, Hf, B.[9-11] This gettering approach, however, requires precise control, since any improved ductility will occur only as long as these second-phase precipitates remain fine; any excessive growth of precipitates, such as the so-called 'Ostwald ripening', would result in an adverse embrittling effect due to the formation of these latent crack starters.

During the recent decade, extensive experimental work was directed at a better understanding of the effect of impurities on brittleness of W. In this respect, a significant contribution of Russian metallurgists should be acknowledged (see, for example, refs 7, 9–14 and references therein). Unfortunately, most of the related papers have been published in Russian and are therefore virtually unknown to metallurgists in the West, though some of the papers have been translated.

Recent progress in developing efficient methods of first-principles calculations and computational algorithms made possible systematic studies of the role of impurities in intergranular cohesion of transition metals at the atomic and the electron-ion level. Calculations using cluster, two-dimensional, and supercell models of GBs with impurities have provided an in-depth insight into mechanisms of GB decohesion (for references, see ref. 15).

Since the first-principles electronic calculations on low-symmetry systems (such as lattice defects or GBs) are still extremely complicated and costly, semi-empirical methods based on strong first-principles foundations have also been developed. Among them, the most popular is the Embedded Atom Method (EAM).[16] This method has been successfully used in a wide variety of calculations.

The purpose of this paper is to elucidate, at the electron–atom level, the energetics of impurities in a tungsten GB and analyze the effect of impurities on W intergranular cohesion. A deeper understanding of the cohesion–decohesion processes at the microscopic level will lay a foundation for 'smart design' of ductile W alloys. In particular, the theoretical analysis of the electron structure and the energetics of W GBs, both clean (CL) and with impurities, enables one to make important predictions. As a result of this theoretical analysis, we suggest a way of improving the W ductility by using the so-called 'site-competition' effect. Boron introduced in minute quantities of 10–50 atomic ppm could cleanse the W GBs of other harmful impurities, enhancing the intergranular cohesion and thus improving the ductility.

ENERGETICS OF IMPURITIES IN W GBs AND THE SITE-COMPETITION EFFECT

In order to study the energetics of impurity atoms in a W GB, we have chosen first to calculate the quantity that may be called the 'environment-sensitive embedding energy' (ESE): the energy of an impurity atom in an atomic environment typical for a GB. Knowledge of these energies for various impurities enables one to compare the relative stability of a particular impurity in the W-GB environment.

Having calculated the ESEs for a number of impurity atoms, one can use this information in a modified EAM approach for calculating the GB relaxation. The latter calculation enables one to draw important conclusions regarding the intergranular cohesion in W in the presence of a specific impurity in the GB.

The model chosen for the GB environment is an eight-atom hexagonal supercell (W_6●, where ● is an impurity atom). The supercell is shown in Fig. 1, together with the capped trigonal-prism coordination of the surrounding W atoms. A trigonal-prism GB configuration is believed to be a typical GB environment in BCC metals and is predicted by the theory of hard-sphere packing. Atomistic-relaxation studies have shown that, in BCC Fe, an impurity atom, such as P or B, is likely to occupy an interstitial position in the center of the trigonal prism formed by Fe atoms in the GB core (even if, as in the case of P and B, the impurity forms a substitutional solid solution with the host). The hexagonal supercell of Fig. 1 has a relatively high symmetry; it also emulates a (111) Σ3 GB environment.[15]

We performed the spin-polarized scalar-relativistic Linear Muffin Tin Orbitals (LMTO) calculations (our method and approximations were the same as in ref. 15). First, a series of calculations (for six different volumes) was performed with an impurity absent from the supercell, i.e. an empty sphere of the same radius as that of the impurity's atomic sphere was substituted for the latter. Similar calculations were then performed for each of the impurities: B, C, N, O, Al, Si, P, and S. The ESEs were defined as follows:

$$\mathrm{ESE} = E(\mathrm{W_6}\bullet) - E(\mathrm{W_6O}) - E(\bullet) \qquad (1)$$

where $E(\mathrm{W_6}\bullet)$ and $E(\mathrm{W_6O})$ are, respectively, the

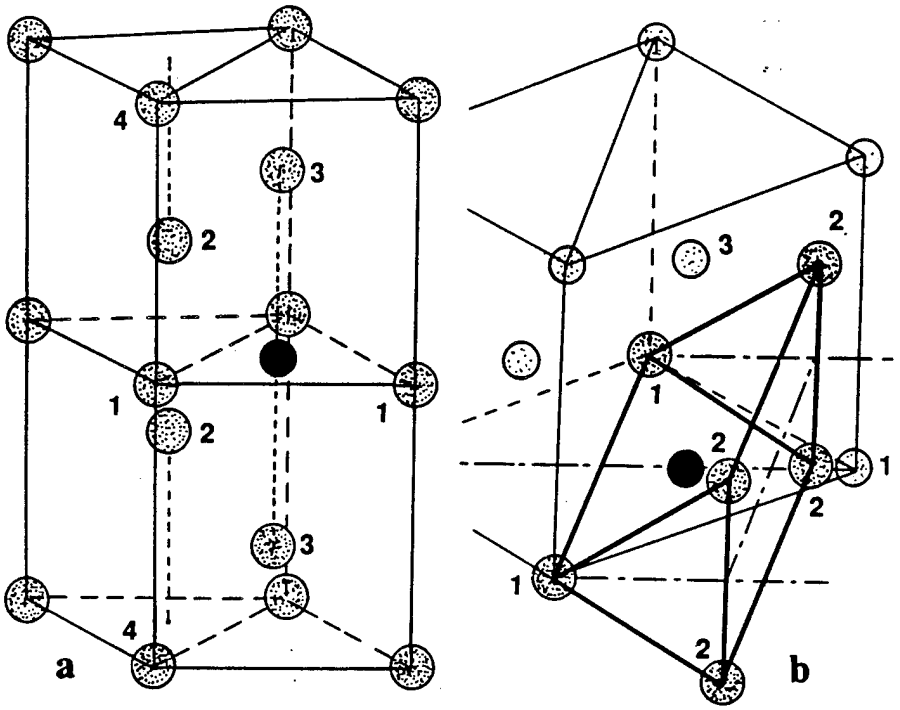

Fig. 1. The W_6● hexagonal supercell emulating a typical trigonal-prism environment of W atoms in the (111) Σ3 FB: (a) the supercell; (b) the trigonal-prism co-ordination; ⊛ W, ● Impurity. Numbers designate atoms W1 to W4.

energies of the supercell with and without the impurity (○ stands for an empty sphere substituted for the impurity atom), and E(●) is the energy of the free impurity atom. In order to make the calculations more consistent, we have chosen to use, as E(●)s, the values of $E(W_6●) - E(W_6○)$ extrapolated to the zero-charge density ($n = 0$), which would correspond to the energy of an impurity in the GB environment with the host crystal lattice infinitely expanded. The ESE energies, eqn (1), as a function of n, the electron-charge density due to W atoms at the impurity site, are presented in Fig. 2.

Plots in Fig. 2 explain an experimentally observed phenomenon known as the 'site-competition' effect. As one can see, in the range of electron-charge density typical of a GB (0·015–0·025 a.u.), B has the lowest energy and thus would tend to displace the other impurities off the GB. Thus there exists a 'site-competition hierarchy'. In fact, in W, N was found to compete successfully over C,[11] while C 'beats' P.[17]

The plots in Fig. 2 also reveal an important aspect of GB-impurity behavior. All the plots have well-pronounced minima. The positions of the minima corresond to the electron density at the impurity site due to the surrounding W atoms that would occur if the GB were allowed to relax in such a way as to minimize the impurity's

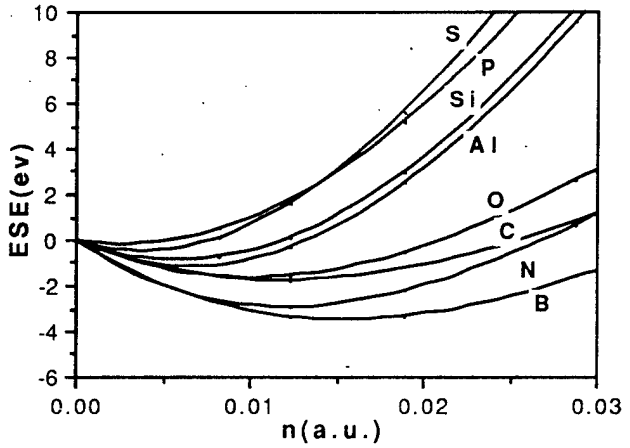

Fig. 2. The 'environment-sensitive embedding energies' plotted against n, the electron-charge density (in atomic units, a.u.).

energy. The minima positions systematically (except for N) shift towards lower densities as the impurity loses its competitive power. A smaller charge density means a 'looser' GB, less strong and more prone to decohesion. The minimization of the total GB energy (rather than only the energy of the impurity atom) gives the characteristic charge densities, which are somewhat higher than those at the minima. However, from this point of view, O, S, P, Si, and Al are the obvious 'decohesion' candidates, whereas B, C, and N may be labeled 'cohesion enhancers'. In

fact, B and C were experimentally found to improve the GB cohesion in W,[9,10,18-20] whereas O, Si, P, and S, known as strong embrittlers,[3,6,17-21] are believed to weaken the GB cohesion.

As mentioned above, the GB environment we were dealing with was that of the (111) Σ3 tilt GB. The GB structure can be represented as a succession of (111) hexagonal planes:

...CBACBACBACB𝔸BCABCABCABC...

(the GB plane is marked by 𝔸). The CB𝔸BC atomic stacking of the core of the GB (CL or with an impurity) is just the one emulated by the eight-atom supercell shown in Fig. 1. In order to find the GB structure corresponding to a minimum of energy, eqn (2), the interplanar distances were varied, whereas the interatomic spacings and the structure within the (111) planes were left unchanged.

The total energy, E, was calculated by using a modified EAM approach:

$$E = \Sigma_R E_{\mathrm{emb}}(n(R)) + (1/2)\Sigma_{R,R'} V(R,R') + \mathrm{ESE}(n(R_{\mathrm{imp}}))$$

where $E_{\mathrm{emb}}(n)$ and $V(R,R')$ are the EAM embedding energy and the pair potential as found for the bulk BCC W (we used the Finnis–Sinclair functions and parameters).[22] The third term is the energy of the impurity atom. The parameters R and R' are the positions of the host atoms, R_{imp} is that of the impurity, and $n(R)$ and $n(R_{\mathrm{imp}})$ are the electron-charge densities at the site of a host atom and the impurity, respectively. The electron-charge density at a given site was taken to be a superposition of the free-atom-charge densities.

As follows from our calculations (Table 2), the volume difference between the CL GB and that with an impurity increases monotonically from B through S. From the intuitive point of view, the increase in volume is expected to result in a weakening of interatomic bonds, though, in principle, an impurity may exert a stronger interaction in spite of the lattice expansion.

Table 2 also shows the interatomic distances in relaxed GBs. The atom designation is shown in Figs 1, 3, and 4. We also number the atomic planes (see below) accordingly: plane 1 (the GB plane) contains atoms W1, plane 2 atoms W2, etc. The distance between an impurity atom (or an empty sphere, O) and W1 atom (2·584 Å), is the same in all cases, since atoms within the (111) planes were not allowed to relax.

The counterpart of the nearest-neighbor distance in the bulk BCC lattice (2·741 Å) is the distance between two W atoms in the (111) direction (W1–W4). In the CL GB, this distance is larger than in the bulk, while the shortest distance is the one between two W2 atoms (W2–W2) across the GB. In the CL GB, there is a significant void (occupied by an O); the distance between W3

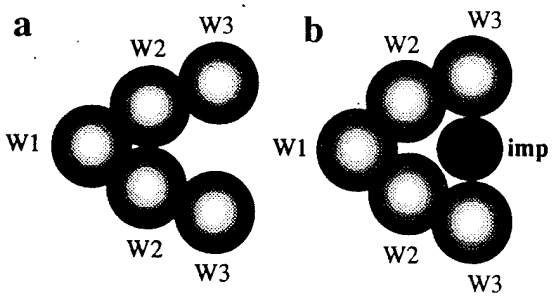

Fig. 3. Arrangement of schematic atomic planes in GB cores: (a) CL GB; (b) GB with an impurity atom.

Table 2. Interatomic distances (in Å) in relaxed GBs, and GB volume-relaxation effect (Å³)*

●	*Distances*				*Volumes*		
	●–W3	*W1–W4*	*W1–W2*	*W2–W2*	Ω	$\Omega-\Omega_{BCC}$	$\Omega-\Omega_{CL}$
O	1·807	2·841	2·873	2·512	148·63	5·95	0
B	2·170	3·056	2·914	2·690	155·28	12·60	6·65
C	2·223	3·090	2·924	2·736	156·48	13·80	7·85
N	2·290	3·133	2·940	2·805	158·12	15·44	9·49
O	2·317	3·150	2·948	2·839	158·80	16·12	10·17
Al	2·539	3·303	3·035	3·182	165·10	22·34	16·47
Si	2·545	3·308	3·037	3·190	165·27	22·41	16·64
P	2·588	3·345	3·048	3·234	166·37	23·69	20·44
S	2·666	3·426	3·090	3·389	169·07	26·39	20·44

*Ω is the volume of nine-layer GB, Ω_{CL} is that of the CL GB, and Ω_{BCC} is the bulk volume per nine atoms, 142·86 Å³; ● is an impurity atom, O is an empty sphere (vacancy).

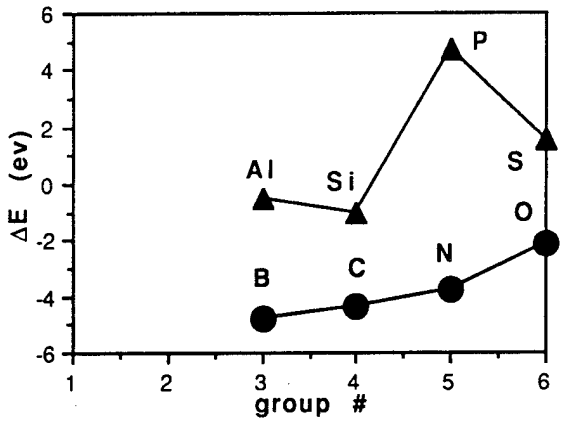

Fig. 4. $\Delta E = E_{GB}(\bullet) - E_{GB}(CL)$, the energy difference between the GB with impurity ● and CL GB, plotted against the periodic-chart group number.

atoms (W3–W3) across the void (and the GB plane) is quite large: 3·614 Å. Thus, in the CL GB, the strongest interaction is W2–W2, followed by W1–W1 and W1–W2. With an impurity atom in place of O, the interatomic interaction changes significantly. Now, the shortest distance is that between an impurity atom and W3, ●–W3, the distance between W2 atoms across the GB being larger. The interaction between the impurity atom and atom W3 becomes of utmost importance. It is actually responsible for the intergranular cohesion: the strongest interaction is exerted between two W3 atoms across the GB via the impurity atom (see Fig. 3). We shall return to this question in the following section.

The GB-relaxation calculations also show that, as in the case of the Fe GB,[23] the interplanar separations oscillate as a function of distance from the GB, the deformation waves decaying by the 10th–12th plane away from the GB. An interesting feature of the CL GB relaxation is that the distance between the 2nd and 3rd planes is a little over a half of the (111) interplanar distance in bulk BCC W (0·550 Å versus 0·914 Å). Though W does not undergo transformation into the ω-phase, the 'misbalance' in interatomic interaction arising as a result of the GB in an attempt to decrease the void volume between two W3 atoms across the GB (see Fig. 3) results in the tendency for plane 3 nearly to collapse onto plane 2 (the ω-phase configuration).

The impurity atoms, B, C, N, and O, result in some 'damping' of the relaxation-deformation waves, i.e. decreasing the oscillation amplitudes. This damping is not pronounced for B and C. Although the distance between planes 1 and 2 (which is half the distance between two atoms in planes 2 across the GB) monotonically increases, the tendency of plane 3 to collapse into plane 2 disappears: in the progression B through O, the distance between planes 2 and 3 is almost equal to that in the bulk. Except for this distance, the amplitude of the deformation waves increases with Al, Si, P, and S.

The analysis of GB energetics reveals only one aspect of an impurity-embrittling effect. From a thermodynamic point of view,[24] the impurity's embrittling potency depends on the difference between the free energies of the impurity's segregation on the initial GB and on the two free surfaces emerging upon fracture. The higher the difference, the stronger is the embrittling potency of the impurity. Thus, in order to have a complete thermodynamic picture of the embrittlement, one should be able to analyze the energetics of the same impurity on the free surface. As a much less rigorous but simpler criterion, the sublimation-energy differences between the host and impurity atoms were calculated by Seah[5] in an ideal-solution model for over 60 elements. According to Seah,[5] among the elements analyzed, only B, C, and Os may be cohesion enhancers in W. In our more rigorous approach, the effects of impurities on GB stability can be analyzed by simply comparing the GB-energy differences, ΔE, between the GB with impurities and the CL GB.

The corresponding values for the impurities discussed are plotted in Fig. 4. One can see that the GB stability decreases from B towards O, and the energy difference becomes positive for P and S—the strongest embrittlers. The latter means that GBs with P and S are unstable at 0 K.

FIRST-PRINCIPLES GB-SUPERCELL CALCULATIONS

In order to study the electronic structure of the GB (both CL and that with an impurity atom in it) we performed a series of LMTO supercell calculations. A 20-atom supercell was used as a model of the GB (Fig. 5). Again as in our semi-empirical calculations, the GB is modeled by the succession of (111) hexagonal planes:

CABCBACBACBABCABCABCABC

The two stacking faults: ...CAC... and ...BAB..., imitate two (111) Σ3 tilt GBs. The filled circles in Fig. 5 show impurity atoms (or empty spheres, if the GB is CL). There are eight planes of W atoms between the two A GB planes. The

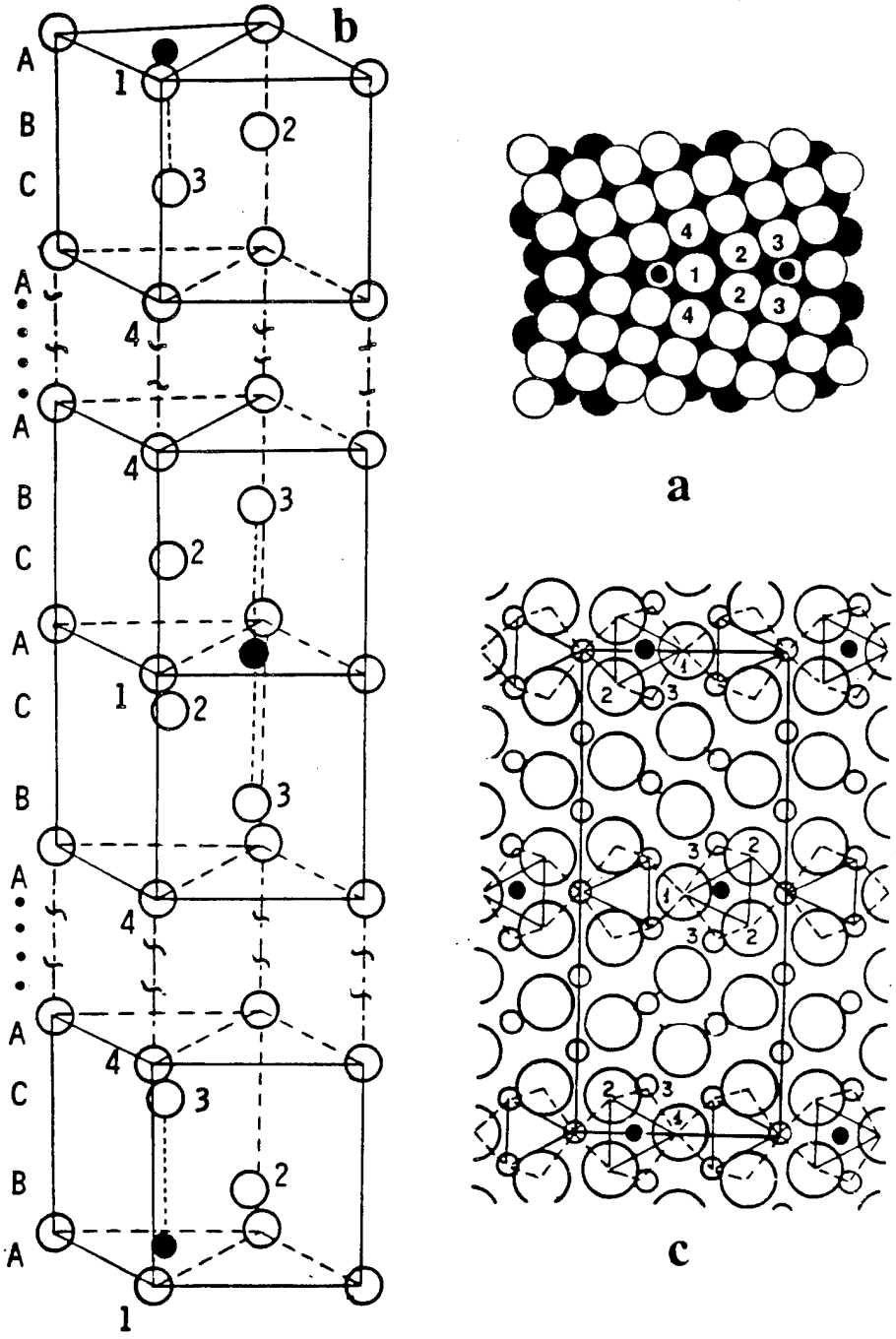

Fig. 5. (a) GB—schematic; (b) 20-atom hexagonal supercell; only parts adjacent to the GBs are shown. As in Fig. 1, numbers designate atoms W1 through W4; (c) view along [112] direction of the periodic (111) plane array; small and large circles are W atoms in alternating (110) planes. Filled circles—impurity atoms (or a vacancy in the case of CL GB).

immediate impurity environment is again the trigonal prism of W atoms shown in Fig. 1.

In order to make the GB model more realistic, the interplanar distances were taken to be equal to those obtained from the above semi-empirical relaxation calculations for planes 2 through 5 (on both sides of the GB planes); the distance between the two equivalent planes in the middle of the supercell was set equal to the interplanar distance in the bulk (0·914 Å).

When a metalloid atom is added into a transition-metal crystal lattice, two effects are produced.[25] First, a covalent bond between the impurity atom and the host transition atom is formed, and then the crystal lattice is expanded and deformed (in fact, both processes occur simultaneously). A similar situation takes place in a W GB.

Figure 6 shows the site-projected electronic densities of states (DOSs) for atoms W1 and W3

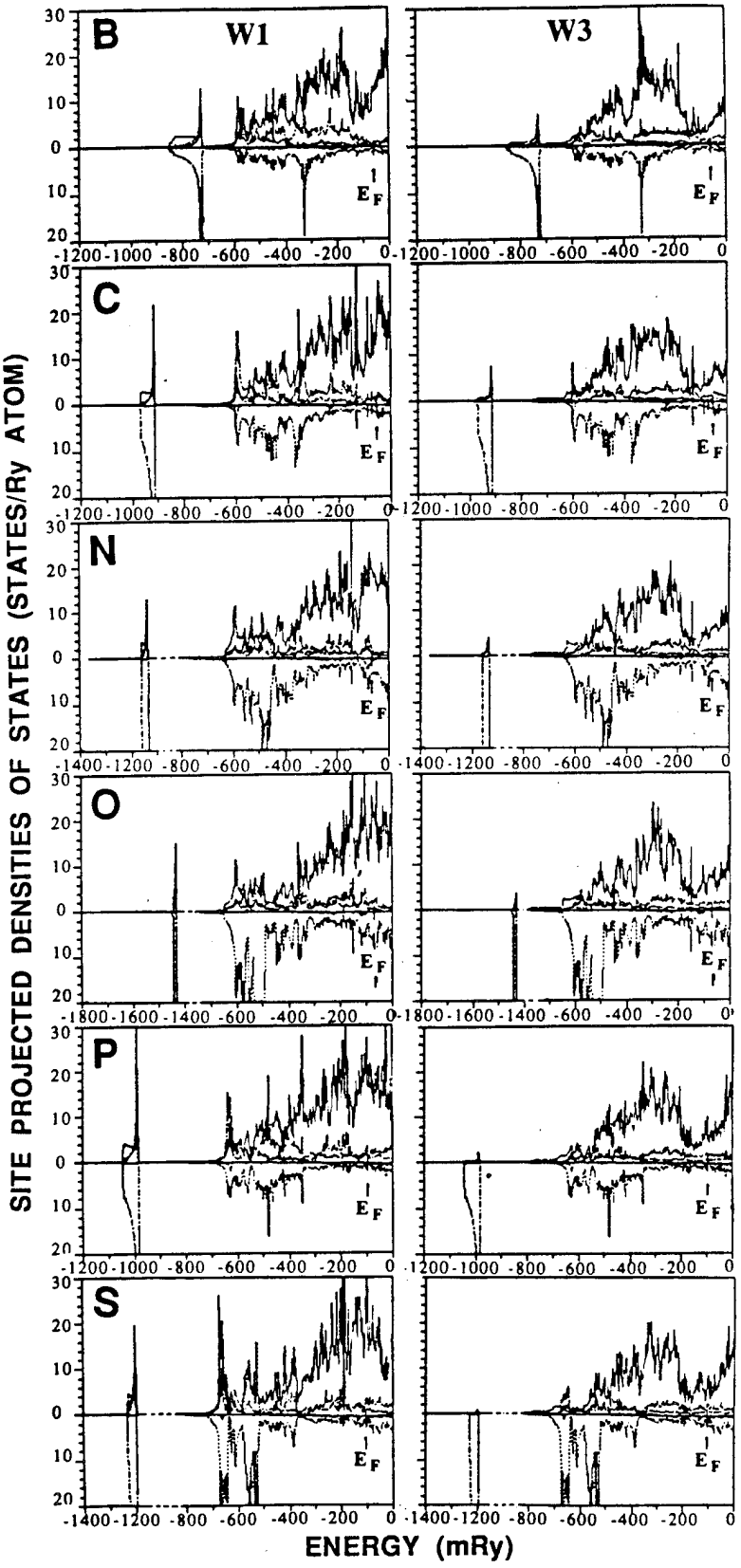

Fig. 6. The site-projected DOSs (states/Ry) for atoms W1 and W3. Zero energy here and in Fig. 8 corresponds to the E_F of bulk BCC W.

for the CL GB and GBs with different impurities. The lower ('negative') parts of the plots show the site-projected DOSs within the atomic spheres of the corresponding impurities; they are identical in plots for W1 and W3 atoms. The plots in Fig. 6 actually represent the GB electronic band structure, and allow an analysis of interatomic bonding.

When an impurity atom is immersed into the electron–atom system of the host, its electrons become part of the whole system. The impurity's electronic states hybridize with the electronic bands of the host metal, which results in the formation of covalent bonds between the impurity and the host atoms. In fact, the whole electron-charge-density distribution becomes affected, and interactions among all the atoms are disturbed.

As is typically the case for metalloid impurities,[15] the impurity *s*-electrons (2*s* for B through O, and 3*s* for P and S) form in W the narrow impurity bands below the bottom of the metal-valence band. Even though the corresponding *s*-levels in the free atoms lie well below the W *p*- and *d*-bands, upon alloying, the *s* electrons do hybridize with those bands, resulting in strongly localized but rather weak ionic-type bonds.

The impurity's *p*-electrons with the energy right inside the W *d*-bands, create pronounced covalent bonds. The impurity-bonding states of predominantly *p*-type hybridize with W mostly *d*- and also *p*-states. Comparison of the DOS plots for W1 and W3 atoms show that the ●–W1 hybridization in the GB plane is stronger than ●–W3 across the GB, in spite of the fact that the former distances are larger than the latter (Table 2). This means that the W atoms in the GB plane are more strongly bound than those across the GB. As one can see, the impurity *s*–*p* bands are shifting towards the W *d*-band bottom, thus 'switching off' the W bonding *d*-electrons in the upper part of the *d*-bands. As a result, the hybridization becomes weaker in the row B through O. In the case of B, a significant part of the W *d*-states is involved. In fact, one can even speculate that the ●–W3 hybridization is the strongest, since a pronounced peak of W *d*-states is involved. For O, P, and S, the hybridization of electronic *d*-states at the bottom of the *d*-band (the peaks around −600 mRy) within the atom W3 sphere almost disappears, while it is still moderate within the atom W1 spheres.

Another important trend can also be seen. Beginning with N and beyond, some anti-bonding states (in both W and ●)—to the right of the 'troughs' around the Fermi energy, E_F—are progressively filled, which results in weakening of the interatomic bonds. In terms of the charge density, 'bonding' means a pile-up of electronic charge in the space between the atoms, whereas the 'anti-bonding' states result in decreasing the charge density. Figure 7 compares the electron-charge densities in atomic spheres of B and O. The arrows show the density values corresponding to the so-called 'muffin-tin' radii, the radii of touching hard spheres representing a B or O and W3 atom (the nearest neighbor to the impurity atoms). One can see that the electron density of B at the 'point of contact' with atom W3 is 1·5 times as great as that of O, which thus suggests a higher 'bonding capacity' of B, as compared with that of O.

Finally, it is interesting to compare the total DOSs of a CL GB, GBs with impurities and bulk BCC W. Figure 8 shows the plots. As in the site-projected DOSs, the GBs with impurities demonstrate strongly localized impurity bands. Each of them contain exactly two electrons, as should be the case, since the corresponding Brillouin zones are completely filled. As was mentioned earlier, the anti-bonding states (to the right of the troughs around ≈ 100 mRy), being almost completely unfilled in bulk W, begin progressively to fill in the GBs. The Fermi energy, E_F, sits on peaks, their heights increasing from B through S. In fact, the E_F peaks in the CL GB is higher than that for B. A relative DOS value at E_F is known to be an indication of the system stability. The higher the value, the lower is the stability. From this point of view, the stability of the GB is lower than that of the bulk W, whereas B improves the stability as compared with that of the CL GB.

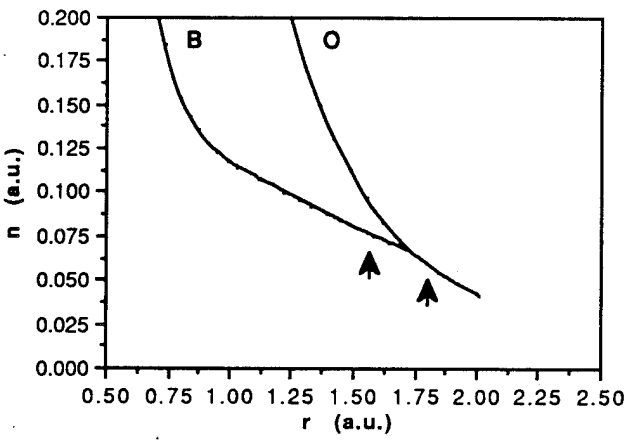

Fig. 7. Electron-charge densities in atomic spheres of B and O.

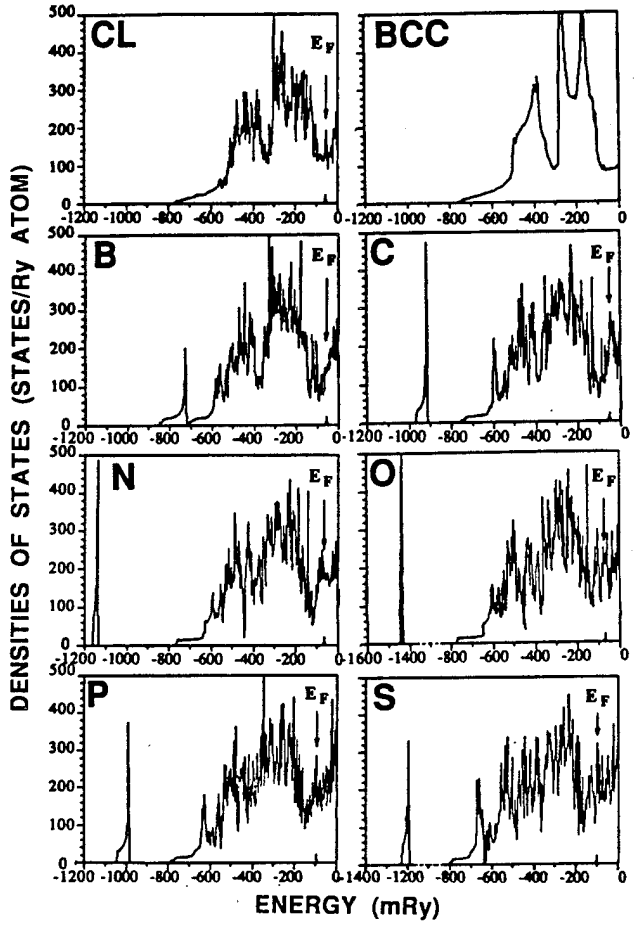

Fig. 8. Total DOSs for BCC W, CL GB, and GB with impurities. Arrows show the Fermi energies.

CONCLUSIONS

Both the semi-empirical and first-principles analyses have shown that B in the W GB plays a dual role. First of all, owing to the site-competition effect, it tends to displace the other impurity atoms off the GB, which thus 'cleanses' it. At the same time, B enhances the intergranular cohesion, which thus improves resistance to brittle fracture. A simple estimate shows that 10–50 ppm of impurity atoms will saturate the GBs in W. Ideally, the same amount of B would be sufficient to improve the ductility significantly. However, the above analysis disregards a possible chemical activity of B, e.g. forming boron oxides or tungsten borides. The latter would require introducing a multiplying factor to correct for B 'consumed' as boron compounds. Alloying W with B in quantities 10–15 times as great did result in a significant (150°C) drop in DBTT.[9,12] This effect was attributed to gettering O by forming boron oxides. In any case, microalloying W with B is extremely promising. The experimental work directed at elucidating the various aspects of microalloying W is currently in progress at the US Army Research Laboratory.

ACKNOWLEDGEMENTS

The author is grateful to Dr R. P. I. Adler and Dr M. Azrin for their interest and invaluable support. Fruitful discussions with Dr R. J. Harrison, R. Dowding, and G. Zilberstein are also gratefully acknowledged. The LMTO code used in calculations was developed by Professor N. Christensen.

REFERENCES

1. Briant, C. L. & Banerji, S. K. (Eds), *Embrittlement of Engineering Alloys*, Academic Press, New York, NY, USA, 1983; Johnson, W. C. & Blakely, J. M. (eds), *Interfacial Segregations*, ASM, Metals Park, OH, USA, 1979.
2. Meyers, C. L., Jr., Onoda, G. Y., Levy, A. V. & Kotfila, R. J., Role of the grain boundaries in the ductile–brittle transition behavior of BCC refractory metals. *Trans. Metall. Soc. AIME*, **233** (1965) 720–8.
3. Joshi, J. & Stein, D. F., Intergranular brittleness studies in tungsten using Auger spectroscopy. *Metall. Trans.*, **1** (1970) 2544–6.
4. Smith, D. A. & Smith, G. D. W., Solute segregations and grain boundary embrittlement of tungsten. In *The Microstructure and Design of Alloys*, Proceedings of the 3rd International Conference on the Strength of Metals and Alloys, London, 1973, pp. 144–8.
5. Seah, M. P., Grain boundary segregation, *J. Phys. F*, **10** (1980) 1043–64; Seah, M. P., Adsorption-induced interface decohesion, *Acta Met.*, **28** (1980) 955–62; Seah, M. P. & Hondros, E. D., Atomistic mechanisms of intergranular embrittlement. In *Atomistics of Fracture*, ed. R. M. Latanision & J. R. Pickens. Plenum, New York, NY, USA, 1983, pp. 855–88.
6. Lee, D. Y., Barrera, E. V., Stark, J. P. & Marcus, H. L., The influence of alloying element on impurity induced grain boundary embrittlement, *Metall. Trans.*, **15A** (1984) 1415–30.

6*a*. Benesovsky, F., Brann, P., Färber, W., Lassuer, E., Petter, H., Tiles, B. & Viehbock, F. P., *Planseeber. Pulvermetallurgie*, **23** (1975) 101–20.

7. Savitskiy, Ye. M. & Burkhanov, G. I., *Physical Metallurgy of Refractory Metals (Metallovedeniye Tugoplavkikh Metallov)*, Nauka, 1967.
8. Wukusick, C. S., The rhenium ductilizing effect. In *Refractory Metals and Alloys. IV: Research and Development*, ed. R. I. Jaffe, G. M. Autl, J. Maltz & M. Semchyshen. Gordon & Breach, New York, NY, USA, 1967, pp. 231–45.
9. Povarova, K. B., Tolstobrov, Yu. O., Popov, A. P. & Konovalov, K. I., Effect of microalloying on the low-temperature plasticity and technological expediency of vacuum-melted tungsten of technical purity, *Izvestiya Akad. Nauk SSSR. Metalliy*, No. 1 (1990) 76–81 (translation: *Russian Metallurgy, Metally*, No. 1 (1990) 74–9).
10. Drachinskii, A. S., Krainikov, A. V., Slyunyaev, V. N. & Trefilov, V. I., Criterion for optimal choice of alloying

elements to lower the intergranular embrittlement in metals of group VIA, *Fizika Metallov i Metallovedenie*, No. 2 (1984) 324–9 (translation: *Phys. Met. Metallogr.*, **58** (1984) 102–7).

11. Burmaka, L. S., Drachinskii, A. S., Ivanchenko, Yu. I., Kostyuchenko, V. G., Trefilov, V. I. & Cherepin, V. T., On the competition between interstitial atoms during the formation of segregates on grain boundaries of molybdenum and tungsten, *Fizika Metallov i Metallovedenie*, **42** (1976) 1089–92 (translation: *Physics of Metals and Metallography*, **42** (1976) 168–71).
12. Povarova, K. B., Drachinskii, A. S., Tolstobrov, Yu. O., Krainkov, A. V., Slyunyaev, V. N., Balashov, V. A., Popov, A. P. & Konovalov, K. I., Effect of microalloying on the ductile–brittle transition temperature of tungsten, *Izvestiya Akad. Nauk SSSR. Metally*, No. 1 (1987) 134–41 (translation: *Russian Metallurgy, Metally*, No. 1 (1987) 129–36); Tolstobrov, Yu. O. & Povarova, K. B., Effect of microalloying with boron on the structure and properties of tungsten, *Fizika i Khimiya Obrabotki Materialov*, **21**(5) (1987) 121–4.
13. Povarova, K. B. & Tolstobrov, Yu. O., The solubility of boron in tungsten, *Izvestia Akad. Nauk SSSR, Metally*, No. 4 (1988) 54–7 (translation: *Russian Metallurgy, Metally*, No. 4 (1988) 52–5); Povarova, K. B. & Zavarzina, E. K., The effect of heat treatment on structure and properties of tungsten alloys, *Izvestia Akad. Nauk SSSR, Metally*, No. 5 (1989) 118–26 (translation: *Russian Metallurgy, Metally*, No. 5 (1989) 112–19).
14. Pavlov, M., Ushakov, Ye. V. & Drobysheva, Ye. Y., *Cold Brittleness and Structure of Tungsten (Khladnolomkost i Struktura Vol'frama)*, Nauka, 1984, pp. 1–129.
15. Krasko, G. L. & Olson, G. B., Effect of boron, carbon, phosphorus and sulfur on intergranular cohesion in iron, *Solid State Commun.*, **76** (1990) 247–51; Effect of hydrogen on the electronic structure of a grain boundary in iron, *Solid State Commun.*, **79** (1991) 113–17.
16. Dow, M. S. & Baskes, M. I., Embedded atom method: derivation and application of impurities, surfaces, and other defects in metals, *Phys. Rev. B*, **29** (1984) 6443–53; Dow, M. S., Model of metallic cohesion: the embedded atom method, *Ibid.*, **39** (1989) 7411–52.
17. Hoffman, H. & Hoffman, S., An AES study of phosphorus and carbon segregation in Ti–Fe-activated sintered tungsten. *Scripta Met.*, **18** (1984) 77–88.
18. Smiti, E., Jouffrey, P. & Kobylanski, A., The influence of carbon and oxygen in the grain boundary on the brittle–ductile transition temperature of tungsten bicrystals. *Scripta Met.*, **18** (1984) 673–6.
19. White, C. L., Keiser, J. R. & Braski, D. N., Boron segregation to grain boundaries and improved ductility in Pt + 30Wt.Pct.Rh + 8Wt.Pct.W. *Metall. Trans.*, **12A** (1981) 1485–90.
20. Taga, H. & Yoshikawa, A., *Proc. ICSTIS, Suppl. Trans. ISIJ*, **11** (1971) 1256–9.
21. Loi, T. H., Morniroli, J. P. & Cantois, M., Segregation of phosphorus at the grain boundaries of polycrystalline tungsten; relations with the brittle–ductile transition temperature and the mode of fracture. In *Physical Chemistry of the Solid State: Application to Metals and Their Compounds*, ed. P. Lacombe. Elsevier, New York, NY, USA, 1984, pp. 243–52; Loi, T. H., Morniroli, J. P., Cantois, M. & Lahaye, M., Brittle fracture of polycrystalline tungsten. *J. Mater. Sci.*, **20** (1985) 199–206.
22. Finnis, M. W. & Sinclair, J. E., A simple empirical N-body potential for transition metals, *Phil. Mag.*, **A50** (1984) 45–56; errata, *ibid.*, **A53** (1986) 161.
23. Krasko, G. L., Environment sensitive embedding energies and grain boundary relaxation in iron. In *Structure and Properties of Interfaces in Materials*, ed. W. A. T. Clark, U. Dahmen & C. L. Briant. *Materials Research Society*, Pittsburgh, PA, USA, 1992, p. 481.
24. Rice, J. R. & Wang, J.-Sh., Embrittlement of interfaces by solute segregations. *Mater. Sci. & Engng*, **A107** (1989) 23–40.
25. Gelatt, C. D., Jr., Williams, A. R. & Moruzzi, V. L., Theory of bonding of transition metals to nontransition metals. *Phys. Rev. B*, **27** (1983) 2005–13.

DISTRIBUTION LIST

No. of Copies	To
1	Office of the Under Secretary of Defense for Research and Engineering, The Pentagon, Washington, DC 20301
	Director, U.S. Army Research Laboratory, 2800 Powder Mill Road, Adelphi, MD 20783-1197
1	ATTN: AMSRL-OP-SD-TP, Technical Publishing Branch
1	AMSRL-OP-SD-TA, Records Management
1	AMSRL-OP-SD-TL, Technical Library
	Commander, Defense Technical Information Center, Cameron Station, Building 5, 5010 Duke Street, Alexandria, VA 23304-6145
2	ATTN: DTIC-FDAC
1	MIA/CINDAS, Purdue University, 2595 Yeager Road, West Lafayette, IN 47905
	Commander, Army Research Office, P.O. Box 12211, Research Triangle Park, NC 27709-2211
1	ATTN: Information Processing Office
	Commander, U.S. Army Materiel Command, 5001 Eisenhower Avenue, Alexandria, VA 22333
1	ATTN: AMCSCI
1	AMCMI-IS-A
	Commander, U.S. Army Materiel Systems Analysis Activity, Aberdeen Proving Ground, MD 21005
1	ATTN: AMXSY-MP, H. Cohen
	Commander, U.S. Army Missile Command, Redstone Arsenal, AL 35809
1	ATTN: AMSMI-RD-CS-R/Doc
	Commander, U.S. Army - ARDEC, Information Research Center, Picatinny Arsenal, NJ 07806-5000
1	ATTN: AMSTA-AR-IMC, Bldg. 59
	Commander, U.S. Army Natick Research, Development and Engineering Center Natick, MA 01760-5010
1	ATTN: SATNC-MI, Technical Library
1	SATNC-AI
	Commander, U.S. Army Satellite Communications Agency, Fort Monmouth, NJ 07703
1	ATTN: Technical Document Center
	Commander, U.S. Army Tank-Automotive Command, Warren, MI 48397-5000
1	ATTN: AMSTA-ZSK
1	AMSTA-TSL, Technical Library
1	AMSTA-SF
	President, Airborne, Electronics and Special Warfare Board, Fort Bragg, NC 28307
1	ATTN: Library

No. of Copies	To
	Director, U.S. Army Research Laboratory, Weapons Technology, Aberdeen Proving Ground, MD 21005-5066
1	ATTN: AMSRL-WT
2	Technical Library
	Commander, Dugway Proving Ground, UT 84022
1	ATTN: Technical Library, Technical Information Division
	Commander, U.S. Army Research Laboratory, 2800 Powder Mill Road, Adelphi, MD 20783
1	ATTN: AMSRL-SS
	Director, Benet Weapons Laboratory, LCWSL, USA AMCCOM, Watervliet, NY 12189
1	ATTN: AMSMC-LCB-TL
1	AMSMC-LCB-R
1	AMSMC-LCB-RM
1	AMSMC-LCB-RP
	Commander, U.S. Army Foreign Science and Technology Center, 220 7th Street, N.E., Charlottesville, VA 22901-5396
3	ATTN: AIFRTC, Applied Technologies Branch, Gerald Schlesinger
	Commander, U.S. Army Aeromedical Research Unit, P.O. Box 577, Fort Rucker, AL 36360
1	ATTN: Technical Library
	U.S. Army Aviation Training Library, Fort Rucker, AL 36360
1	ATTN: Building 5906-5907
	Commander, U.S. Army Agency for Aviation Safety, Fort Rucker, AL 3636
1	ATTN: Technical Library
	Commander, Clarke Engineer School Library, 3202 Nebraska Ave., N., Fort Leonard Wood, MO 65473-5000
1	ATTN: Library
	Commander, U.S. Army Engineer Waterways Experiment Station, P.O. Box 631, Vicksburg, MS 39180
1	ATTN: Research Center Library
	Commandant, U.S. Army Quartermaster School, Fort Lee, VA 23801
1	ATTN: Quartermaster School Library
	Naval Research Laboratory, Washington, DC 20375
1	ATTN: Code 6384
	Chief of Naval Research, Arlington, VA 22217
1	ATTN: Code 471
	Commander, U.S. Air Force Wright Research and Development Center, Wright-Patterson Air Force Base, OH 45433-6523
1	ATTN: WRDC/MLLP, M. Forney, Jr.
1	WRDC/MLBC, Mr. Stanley Schulman

No. of Copies	To
	U.S. Department of Commerce, National Institute of Standards and Technology, Gaithersburg, MD 20899
1	ATTN: Stephen M. Hsu, Chief, Ceramics Division, Institute for Materials Science and Engineering
1	Committee on Marine Structures, Marine Board, National Research Council, 2101 Constitution Avenue, N.W., Washington, DC 20418
1	Materials Sciences Corporation, Suite 250, 500 Office Center Drive, Fort Washington, PA 19034
1	Charles Stark Draper Laboratory, 555 Technology Square, Cambridge, MA 02139
	General Dynamics, Convair Aerospace Division, P.O. Box 748, Fort Worth, TX 76101
1	ATTN: Mfg. Engineering Technical Library
	Plastics Technical Evaluation Center, PLASTEC, ARDEC, Bldg. 355N, Picatinny Arsenal, NJ 07806-5000
1	ATTN: Harry Pebly
1	Department of the Army, Aerostructures Directorate, MS-266, U.S. Army Aviation R&T Activity - AVSCOM, Langley Research Center, Hampton, VA 23665-5225
1	NASA - Langley Research Center, Hampton, VA 23665-5255
	U.S. Army Vehicle Propulsion Directorate, NASA Lewis Research Center, 2100 Brookpark Road, Cleveland, OH 44135-3191
1	ATTN: AMSRL-VP
	Director, Defense Intelligence Agency, Washington, DC 20340-6053
1	ATTN: ODT-5A, Mr. Frank Jaeger
	U.S. Army Communications and Electronics Command, Fort Monmouth, NJ 07703
1	ATTN: Technical Library
	U.S. Army Research Laboratory, Electronic Power Sources Directorate, Fort Monmouth, NJ 07703
1	ATTN: Technical Library
	Director, U.S. Army Research Laboratory, Watertown, MA 02172-0001
2	ATTN: AMSRL-OP-WT-IS, Technical Library
5	Author

Accession For
NTIS GRA&I ☑
DTIC TAB ☐
Unannounced ☐
Justification
By
Distribution/
Availability Codes
Dist | Avail and/or Special
A-1 | 20